Late spring frost delays tree spring phenology by reducing photosynthetic productivity

Jinmei Wang[1]†, Hao Hua[2]†, Jing Guo[1]†, Xu Huang[1], Xin Zhang[1], Yuchuan Yang[1], Danying Wang[1], Xiali Guo[3], Rui Zhang[4], Nicholas G. Smith[5], Sergio Rossi[6], Josep Peñuelas[7,8], Philippe Ciais[9], Chaoyang Wu[2]*, Lei Chen[1]*

[1]Key Laboratory of Bio-Resource and Eco-Environment of Ministry of Education, College of Life Sciences, Sichuan University, Chengdu, 610041, China.

[2]Key Laboratory of Land Surface Pattern and Simulation, Institute of Geographical Sciences and Natural Resources Research, Chinese Academy of Sciences, Beijing, China.

[3]State Key Laboratory for Conservation and Utilization of Agro-bioresources, Guangxi Key Laboratory of Forest Ecology and Conservation, College of Forestry, Guangxi University, Nanning 530004, China

[4]State Key Laboratory of Subtropical Silviculture, Zhejiang A&F University, 666 Wusu Street, Hangzhou 311300, China.

[5]Department of Biological Sciences, Texas Tech University, Lubbock, Texas 79409, USA.

[6]Département des Sciences Fondamentales, Université du Québec à Chicoutimi, Chicoutimi, G7H 2B1, Canada.

[7]Global Ecology Unit Center for Ecological Research and Forestry Applications (CREAF)-National Research Council (CSIC)-Universitat Autonoma de Barcelona (UAB), National Research Council (CSIC), Bellaterra, Catalonia 08194, Spain.

[8]Center for Ecological Research and Forestry Applications (CREAF), Cerdanyola del Vallès, Barcelona, Catalonia 08193, Spain

[9]Laboratoire des Sciences du Climat et de l'Environnement, LSCE/IPSL, CEA-CNRS- UVSQ, Université Paris-Saclay, Gif-sur-Yvette, France.

† These authors contributed equally to this work

*Corresponding authors:
Chaoyang Wu, wucy@igsnrr.ac.cn;
Lei Chen, lei.chen1029@gmail.com

Abstract

Under climate warming, earlier spring phenology has heightened the risk of late spring frost (LSF) damage. However, the intricate interplay among LSF, spring phenology, and photosynthetic carbon uptake remains poorly understood. Utilizing 286,000 ground phenological records involving 870 tree species and remote-sensing data across the Northern Hemisphere, we show that LSF occurrence in a given year reduces photosynthetic productivity by 13.6%, resulting in a delay in spring phenology by approximately 7.0 days in the subsequent year. Our experimental evidence, along with simulations using modified process-based phenology models, further supports this finding. This frost-induced delay in spring phenology subsequently leads to a decrease in photosynthetic productivity during the next year following an LSF event. Therefore, it is essential to integrate this frost-induced delay in spring phenology into current Earth System Models to ensure accurate predictions of the impacts of climate extremes on terrestrial carbon cycling under future climate change.

Main

Tree phenological events, encompassing seasonal biological activities like budbreak and leaf-out, wield substantial influence over carbon, water, nutrient cycling, and trophic interactions within forest ecosystems[1,2]. Late spring frost (LSF), characterized by frost events taking place during or after leaf emergence, emerges as a significant threat to tree growth and the functionality of forest ecosystems[3–5]. Trees undergo deep physiological dormancy, termed endodormancy, during winter, which maximizes frost resistance until adequate chilling units accumulate. As spring arrives, trees transition to ecodormancy, accompanied by diminishing freezing resistance and the emergence of new leaves, marking the lowest freezing resistance[6]. The occurrence of LSF after leaf-out can inflict severe harm upon these nascent leaves[7,8]. Hence, trees strive to initiate leaf growth as early as possible, optimizing the production of photosynthetic carbohydrates while sidestepping the perils of LSF[9,10]. The past decades have witnessed the propagation of earlier spring phenology due to global warming across the Northern Hemisphere[11–13]. This warming-induced advancement in spring phenology contributes to extended carbon assimilation periods but also heightens the risk of LSF[14–16]. Consequently, it becomes imperative to comprehend and model the intricate dynamics between LSF, tree productivity, and climate change to establish effective forest management strategies.

Sufficient carbon assimilation and storage during the prior growing season are vital for winter survival and supporting early spring leaf growth[17,18]. Nonstructural carbohydrates (NSC), including soluble sugars and starch, peak in autumn before dormancy but dwindle after new leaves emerge in spring[19,20]. Frost events amplify stem respiration, intensify carbon depletion, and trigger the formation of ice crystals, potentially damaging biomembranes and dehydrating cells, ultimately diminishing stored carbon reserves[7,21]. A significant drop in carbon assimilation renders available carbon reserves inadequate for fueling the energy and osmotic needs of leaf-out[22,23]. Consequently, more chilling or forcing units might be needed to initiate spring leaf-out, leading to delayed spring phenology[22,23]. LSF may disturb the uptake of photosynthetic carbon and impact the accumulation of chilling and forcing units as supplementary energy sources, thus influencing spring phenology in the subsequent year. However, the interactions between frost, carbon uptake, and phenology spanning multiple growing seasons in trees have remained largely unexplored.

In this study, we endeavor to unravel the intricate interplay between LSF, photosynthetic productivity, and spring phenology across the Northern Hemisphere by combining multiple complementary long-term and large-scale datasets and frost-controlled experiments. Specifically, we embark on deciphering the carry-over effect of LSF on subsequent-year spring phenology and photosynthetic productivity across subtropical, temperate, and boreal regions in the Northern Hemisphere. Our hypothesis postulates that the reduction in carbon uptake due to frost triggers an augmented demand for (1) chilling units, (2) forcing units, or (3) both, thereby delaying the onset of spring phenology in the subsequent year. This frost-induced delay, in turn, would decrease productivity through a feedback process.

Carry-over effect of LSF on spring phenology

To investigate the carry-over effect of LSF on spring phenology, we compiled leaf-out records of 870 tree species spanning from 1950 to 2020. These records were sourced from five large-scale ground-based phenological and PhenoCam networks situated in Europe, the USA, China, and Russia, spanning diverse climate zones within the Northern Hemisphere (Fig. 1a). The leaf-out dates were employed to denote the start of season (SOS) and LSF events were defined as occurrences of daily minimum temperatures dropping below −2°C after the SOS. We test the impact of LSF on SOS, and computed the difference in SOS (ΔSOS) for consecutive two-year periods, per species at each site. Subsequently, we contrasted the differences in ΔSOS when LSF transpired versus when it did not, for each species at each site. Positive and negative values of ΔSOS indicated delayed and advanced SOS in the subsequent year (SOS_{next}) relative to the present year ($SOS_{current}$). Through the utilization of ground-based phenological networks, we found that, in the absence of LSF, the mean ΔSOS remained close to zero, while it was positive (5.70 ± 0.06 days) during LSF occurrences (Fig. 1b). This observation indicated a significant delay in SOS_{next} attributable to LSF in the current year. Similar results were obtained across diverse ground-based phenological networks and through analysis using linear mixed models (Supplementary Fig. 1 and Supplementary Table 1).

Generalizing our findings, we calculated ΔSOS based on phenological metrics obtained from GIMMS NDVI3g and MODIS datasets spanning 1982 to 2019 (Fig. 1c–h). The analysis employing GIMMS NDVI3g highlighted that 85.7% of forested areas depicted earlier SOS_{next}, indicated by negative ΔSOS values, when LSF did not occur in the Northern Hemisphere (Fig. 1c). Conversely, in the presence of LSF, 90.6% of forested areas displayed delayed SOS_{next} (Fig. 1d). These trends were consistent when utilizing the MODIS data (Fig. 1f, g). On the whole, SOS_{next} was found to advance by 2.30 ± 0.01 days when LSF was absent, whereas it exhibited a delay of 7.18 ± 0.03 days when LSF was present (Fig. 1e, h). To ensure the robustness of our results, we further excluded the influence of preseason temperatures on spring phenology (see Methods). We also observed that SOS_{next} was delayed by LSF after excluding the effect of spring temperature (Supplementary Fig. 2 and Supplementary Table 2).

Analogous outcomes were evident across diverse tree species, forest types, and climate zones, as inferred from both ground-based phenological datasets and remote sensing data (Fig. 2a, b and Supplementary Figs. 3–5). The observed delay in SOS_{next} was significantly more pronounced in broadleaf tree species compared to conifer species and in late-leafing species compared to early-leafing species (Fig. 2a, b). Additionally, we observed a significant escalation in frost-induced delayed SOS_{next} as the severity of LSF heightened across various species (Extended Data Fig. 1). To assess the robustness of our results, we also examined the impact of LSF occurring one to eight weeks after SOS and before July 15th on SOS_{next} using a one-week smoothing window. Consistently, we observed a delay in SOS_{next}, regardless of the temperature thresholds or timing of LSF occurrence (Supplementary Fig. 6). Moreover, we found that the delay in SOS_{next} due to frost was more pronounced when LSF occurred later compared to earlier in the season. The risk of LSF was also higher for later occurrences compared to earlier ones (Supplementary Fig. 7).

Species-specific phenological responses to LSF

To glean greater clarity about disparities in the response of SOS_{next} to LSF across tree species, we calculated the lethal temperature at which 50% of leaves were impaired (LT_{50}). We selected long-term and extensive SOS records from the PEP725 network for the calculation of LT_{50}. The LT_{50} was estimated for all eight species, based on median SOS dates for each species within the PEP725 dataset and six experimentally derived LT_{50} values from pertinent literature sources (Supplementary Table 3). We observed a strong positive correlation between measured and predicted LT_{50} values (Supplementary Fig. 8). The outcomes revealed an LT_{50} range of −8°C to −2°C across the eight species, with early-leafing species exhibiting a significantly lower LT_{50} than their late-leafing counterparts (Fig. 2c). Employing linear regression, a positive linear correlation was evident between LT_{50} and ΔSOS for consecutive two-year periods (Fig. 2d).

This finding suggested that tree species with low frost resistance experienced a more pronounced delay in SOS_{next} compared to those with high frost resistance when LSF occurred.

Interactions between LSF, phenology and productivity

To expound upon the frost-induced alterations in SOS_{next}, we examined the discrepancies in gross primary productivity (GPP) and net primary productivity (NPP) when LSF occurred or did not. We found the GPP of the current year ($GPP_{current}$) decreased by 13.6% when LSF occurred (Fig. 3a, b). We obtained similar results utilizing remote-sensing vegetation indices and tree-ring width in the Northern Hemisphere (Supplementary Figs. 9 and 10). To investigate the effect of LSF on photosynthetic carbon uptake, we conducted frost experiments using seedlings of four widely distributed tree species in subtropical and temperate forests (see Methods). Our findings revealed a significant decrease in leaf photosynthetic rate, starch, soluble sugar, and NSC in tree seedlings when LSF occurred (Fig. 3c–j and Supplementary Figs. 11–14). These results provide experimental evidence that LSF significantly reduces leaf photosynthetic rate and carbon storage.

To bolster these findings, a piecewise structural equation model (SEM) was constructed to probe the direct and indirect effects of LSF on $GPP_{current}$ and SOS_{next}. The SEM outcomes unveiled a negative correlation between LSF and $GPP_{current}$ (Fig. 3k, l and Supplementary Table 4), affirming the substantive reduction in $GPP_{current}$ caused by LSF. Additionally, SOS_{next} exhibited positive correlations with LSF and SOS in the current year ($SOS_{current}$), while demonstrating a negative correlation with $GPP_{current}$. This finding indicated that a decline in $GPP_{current}$ led to a delayed SOS_{next}. Consequently, the SEM elucidated that LSF exerted a dampening effect on $GPP_{current}$, thereby contributing to the postponement of SOS_{next}. Analogous outcomes were discerned within $NPP_{current}$ (Supplementary Fig. 15 and Supplementary Table 5). In addition, we found a significant decrease in $GPP_{current}$ when LSF occurred in both drought and non-drought years (Extended Data Fig. 2).

To unravel the mechanisms underpinning the correlation between frost-induced carbon reduction and subsequent-year spring phenology, we postulated that trees would necessitate additional chilling units, forcing units, or a combination thereof, to initiate spring phenology following decreased carbon assimilation in the preceding year. To test these hypotheses, a range of process-based spring phenological models were modified by integrating the impact of LSF-induced GPP reduction on spring phenology (see Methods). We found that the modified phenology models outperformed their respective original versions, and the modified two-phase sequential model (SM), specifically adjusted in the forcing phase, emerged as the optimal model for simulating spring phenology (Fig. 3m–p).

Projected impact of LSF on future spring phenology

Using the modified SM, we predicted shifts in spring phenology during LSF occurrences and compared these simulations with projections from temperature-driven CMIP6 models under diverse future emission scenarios (see Methods). We found that, in the absence of LSF, the mean ΔSOS was negative (−1.70 ± 0.02 days) (Fig. 4). However, when LSF events occurred, the mean ΔSOS remained close to zero (0.67 ± 0.01 days) across all four climatic scenarios simulated by CMIP6 models. Using the modified SM, we found that the mean ΔSOS became positive (5.27 ± 0.03 days) in the presence of LSF under all four future climatic scenarios, with the highest mean ΔSOS (7.33 ± 0.07 days) observed under the high-emission SSP5-8.5 scenario (Fig. 4i–l). To reduce uncertainties arising from relying on a single phenological dataset, we further performed the same analysis using daily leaf area index (LAI) data from CMIP6 models under four future climatic scenarios, and obtained consistent results (Supplementary Fig. 16). Furthermore, utilizing data from all ground-based phenological networks, we observed a rising trend in the mean SOS_{next} attributed to LSF between 1950 and 2020, accompanied by an increased LSF risk (Extended Data Fig. 3 and Supplementary Fig. 17). These analyses highlight that the CMIP6 models underestimated the delaying impact of LSF on spring phenology under future emission scenarios.

Interactions between LSF, phenology, and productivity

To decipherer the interactions between LSF, SOS, and productivity, we further examined the impact of LSF on the GPP in the next year (GPP_{next}) when LSF occurred. Results showed that GPP_{next} decreased by 11.2 % when LSF occurred (Extended Data Fig. 4a, b). Furthermore, we observed significantly higher ΔGPP_{next} values when SOS_{next} was advanced, irrespective of LSF occurrence (Extended Data Fig. 4e, f). Conversely, no substantial disparities were apparent in ΔGPP_{next} when LSF events transpired or not, regardless of the advancement or delay in SOS_{next}. Similar trends were observed within NPP_{next} (Extended Data Fig. 4c, d, g and h). This suggested that changes in GPP_{next} and NPP_{next} were closely linked to the timing of SOS_{next}.

Discussion

In addition to the warming-induced earlier spring phenology, the risk of LSF is also increasing[16,24–26]. Numerous studies have demonstrated that LSF can severely damage newly developed buds and leaves of trees[7,8]. However, the carry-over effect of LSF on vegetation growth and productivity has been largely neglected. By combining multiple long-term and large-scale ground and remote sensing datasets, we discovered that the onset of spring phenology was significantly delayed in the year following an LSF event, resulting in reduced carbon assimilation in the subsequent year. Furthermore, our results suggested that the delayed spring phenology in the subsequent year, induced by LSF, was driven by reduced carbon uptake in the year of occurrence. As a consequence, photosynthesis was reduced for two years following an LSF event (Fig. 5).

Effect of LSF on spring phenology

In winter and spring, trees typically undergo periods of endodormancy and ecodormancy before initiating spring growth[27]. Trees need to accumulate chilling units (i.e., cold temperatures) to fulfill endodormancy, while the accumulation of forcing units (i.e., warm temperatures) is necessary to break ecodormancy[13]. Warming springs can lead to earlier spring phenology by accelerating the accumulation of forcing units required for trees to end dormancy[12,28]. However, trees also need to assimilate and store adequate carbohydrates through photosynthesis to maintain metabolic processes during dormancy, protect cells from winter freezing damage, and support bud development and early spring leaf growth in cold regions[17,18,29]. When occurring after leaf-out, frost events can decrease photosynthetic pigments (e.g., chlorophyll), and even lead to complete and irreversible damage to photosynthesis and photosystems, resulting in decreased carbon uptake[30–32]. Our analysis, based on multiple data sources and frost-controlled experiments, provides direct and robust evidence that LSF can significantly impact the photosynthetic carbon uptake of trees.

If trees experience a significant decline in carbon assimilation when LSF occurs, available carbon reserves might be insufficient to fulfill the energetic and osmotic requirements to support the growth of buds and leaves[22,23,33]. Consequently, trees may adopt a conservative strategy to reduce and avoid the risk of frost damage, resulting in longer periods of deep physiological dormancy and ecodormancy. When LSF occurs, ending the prolonged and deep dormancy period requires greater accumulations of chilling units, forcing units, or both in order to compensate for the carbon loss, ultimately leading to a delayed spring leaf-out in the following year. Therefore, LSF in a given year may delay spring phenology in the following year by altering the accumulation of chilling and forcing units required for trees to break dormancy. To provide explanations for the delayed spring phenology in the subsequent year due to frost-induced carbon reduction, therefore, we proposed three hypotheses: the reduced carbon uptake would lead to an increase in the requirements of (i) chilling units, (ii) forcing units, or (iii) both chilling and forcing units to trigger the onset of spring phenology. To test these hypotheses, we modified a series of process-based phenological models by incorporating the effect of frost-induced decrease in carbon assimilation on spring phenology. We observed that the modified process-based phenology model, with adjustments applied solely in the forcing phase, showed superior performance compared to other models. This finding suggests that, in order to supplement carbon loss, trees might require higher forcing units as an additional energy source to trigger the onset of spring leaf-out. This trade-off between carbon uptake and forcing units well explains the observed delay in spring phenology in the subsequent year when LSF occurred. By integrating various complementary data sources and conducting an additional frost-controlled experiment, our study provides compelling evidence that LSF can significantly postpone spring phenology in the following year by decreasing photosynthetic carbon assimilation in the current year.

Projected LSF effect on spring phenology

The global average temperature is projected to rise by around 2°C to 4°C within this century, increasing the risk of LSF[34]. However, we found that CMIP6 models underestimate the effect of LSF on spring phenology under future climate warming. Although the impact of LSF on vegetation growth has recently been incorporated into Dynamic Global Vegetation Models (DGVMs)[35–37], the phenological response to frost events is not yet coupled in Earth System Models (ESMs). Therefore, ESMs have limitations in accurately depicting extreme events and their impacts on vegetation phenology. Due to the absence of intricate interactions between carbon uptake and spring phenology, traditional ESMs fail to detect and even underestimate the delaying effect induced by LSF[38]. In contrast, our modified phenology model incorporates the impact of LSF-induced carbon loss, significantly enhancing the simulation of projected delays in spring phenology under future climatic scenarios. By integrating the interactions among LSF, carbon assimilation, and spring phenology, our modified phenology model offers a novel and comprehensive framework for understanding and predicting changes in spring phenology and terrestrial carbon cycling in a warming world.

Variation among tree species and regions

We observed that the magnitude of the delayed effect of LSF in the current year on spring phenology in the next year varied among different tree species and regions. Specifically, spring phenology of broadleaf tree species was delayed more than that of conifer tree species. It is reported that thick and narrow needles in conifers are often more resistant to extreme climate conditions, such as frost and drought, compared to wide and flat leaves in broadleaf trees[39,40]. Broadleaf tree species are therefore more vulnerable to frost damage compared to conifer tree species. In addition, conifer trees carry multiple generations of needles, and old needles could compensate for photosynthesis once new needles are damaged by frost[41]. The clade-specific foliar traits may explain why spring phenology in conifers is less sensitive to frost than it is in broadleaved trees.

Early-leafing species often exhibit an “opportunistic” strategy to maximize photosynthetic carbon assimilation despite the risk of frost damage, compared to late-leafing species that are more sensitive to photoperiod[16,42,43]. We observed that spring phenology of late-leafing species in the next year was delayed more than that of early-leafing species when LSF occurred. Generally, species that leaf emergence occurred earlier experience a higher risk of frost damage compared to late-leafing species. Therefore, early-leafing species might have evolved a higher frost resistance to reduce the damage when LSF occurred. To test this hypothesis, we further examined the relationship between frost resistance, indicated by the LT_{50}, and the timings of leaf-out in eight widely distributed temperate broadleaf tree species. Our results indicated that species with earlier leaf-out had a significantly stronger frost resistance than those with later leaf-out. Moreover, frost-induced delayed days of spring phenology showed a significant decrease with an increase in frost resistance. Therefore, species-specific frost resistance well explains why the early-leafing species are less sensitive to frost compared to the late-leafing species.

Combining long-term and large-scale ground-based phenological records across the Northern Hemisphere, we found that LSF significantly delayed spring phenology in the subsequent year by reducing photosynthetic carbon assimilation. This conclusion was further reinforced by the evidence gathered from our frost-controlled experiment and the simulations of process-based phenology models. We further observed a significant decrease in GPP in the subsequent year due to the frost-induced delay in spring phenology, indicating the feedback effect of frost-induced delay in spring phenology on GPP. Our results reveal complex interactions between spring-frost risk, phenology, and terrestrial carbon cycling. In light of the increasing risk of LSF, it is crucial to integrate our findings into Earth System Models to ensure accurate projections of the impact of climate extremes on terrestrial carbon cycling under future climate change, which can further inform decision-making regarding the ecological and economic impacts of these frost events on land management, forestry, and agriculture.

Acknowledgments

We are grateful to Dr. Constantin M. Zohner, Yann Vitasse, and Ivan Janssens for helpful comments on this project. L.C. was funded by National Natural Science Foundation of China (32271833) and National Key R&D Program of China (2023YFF0806600). C.W. was funded by National Natural Science Foundation of China (42125101). J.P. was funded by the Spanish Government grants TED2021-132627 B–I00 and PID2022-140808NB-I00, funded by MCIN, AEI/10.13039/ 501100011033 European Union Next Generation EU/PRTR, the Fundación Ramón Areces grant CIVP20A6621, and the Catalan Government grant SGR 2021–1333.

Author contributions

L.C. and C.W. designed the research. J.W., J.G. and H.H. performed the data analysis. J.G. and J.W. wrote the paper with the inputs of H.H., X. H., X. Z., Y.Y., D.W., X. G., N.G.S., S.R., J.P., P.C., C.W. and L.C. All authors contributed to the interpretation of the results, and approved the final manuscript.

Competing interests

The authors declare no competing interests.

Fig. 1 | Effect of late spring frost (LSF) on start of growing season (SOS) in the next year. **a**–**h**, Locations of the ground-based phenological and PhenoCam network sites **(a)**, changes in ΔSOS between LSF occurred and non-occurred across all phenological networks, Pan European Phenology Network (PEP725), USA National Phenology Network (USA-NPN), China Phenological Observation Network (CPON), Russian 'Chronicles of Nature' Network (RCNN), and PhenoCam network **(b)**, spatial distribution of mean ΔSOS from phenological products of GIMMS NDVI3g **(c**, **d)** and MODIS **(f**, **g)** when LSF non-occurred **(c**, **f)** and occurred **(d**, **g)** over the Northern Hemisphere forests, and changes in ΔSOS between LSF occurred and non-occurred from phenological products of GIMMS NDVI3g **(e)** and MODIS **(h)**. In **b**–**h**, ΔSOS indicates difference in SOS for each consecutive two-year period at each site or pixel. In **b**, **e** and **h**, the Y and N indicate LSF occurred or did not in each year for each species at each site (pixel), respectively. Statistical significance between groups was determined using two-tailed t test. The asterisk indicates a significant difference in ΔSOS between LSF occurred and non-occurred ($P < 0.01$). The box spans from the first to the third quartile, with intermediate values marked as the black line in the middle of the box. In **c**, **d**, **f** and **g**, the histograms present the frequency distributions of the percentages.

Fig. 2 | Effect of late spring frost (LSF) on start of growing season (SOS) in the next year for broadleaf and conifer species, and for early- and late-leafing species. **a**,**b**, Changes in ΔSOS between broadleaf and conifer species **(a)**, and between early- and late-leafing species **(b)** when LSF occurred or did not using ground-based phenological networks. **c**,**d**, The LT_{50} searched and compiled from literature data for species of PEP725 dataset and predicted by the four-parameter logistic model based on the median dates of leaf-out **(c)**, and the linear relationship between the predicted LT_{50} and ΔSOS **(d)**. In **a**, **b** and **d**, ΔSOS indicates difference in SOS for each consecutive two-year period for each species at each site. In **a** and **b**, the Y and N indicate LSF occurred or did not in each year for each species at each site, respectively. Statistical significance was determined using two-tailed t test. The asterisk indicates a significant difference in ΔSOS between groups ($P < 0.01$). The box spans from the first to the third quartile, with intermediate values marked as the black line in the middle of the box. In **c** and **d**, black and red dots represent the LT_{50} collected in the literature and predicted by the four-parameter logistic model, respectively. The black lines represent fits from a four-parameter logistic model in **c** and a linear regression model in **d**, respectively. The shading represents 95% confidence interval.

Fig. 3 | Relationships between late spring frost (LSF), spring phenology, and photosynthetic productivity. **a**,**b**, Changes in annual gross primary productivity in the current year ($GPP_{current}$) between LSF occurred and non-occurred using phenological products of GIMMS NDVI3g **(a)** and MODIS **(b)**. **c**–**f**, Changes in photosynthetic rate (**c**), starch (**d**), soluble sugar (**e**), and nonstructural carbohydrates (**f**) across all tree species in control (CK) and LSF group. **g**–**j**, LSF treatment using seedlings from four tree species. **k**,**l**, Piecewise structural equation model (SEM) considering both LSF and $GPP_{current}$ using phenological products of GIMMS NDVI3g **(k)** and MODIS **(l)**. **m**–**p**, The percentages of pixels with significant correlations (Freq) (**m**), average correlation coefficient (*R*) (**n**), Root Mean Square Error (RMSE) (**o**), and Kling-Gupta Efficiency (KGE) (**p**) between model estimates and satellite-derived observations using the growing degree days (GDD), spring warming (SW), sequential model (SM), parallel model (PM), and corresponding modified models with GPP effects. In **a** and **b,** the Y and N indicate LSF occurred or did not in each year at each pixel, respectively. Statistical significance was determined using two-tailed t test. The asterisk indicates a significant difference in $GPP_{current}$ between LSF occurred and non-occurred ($P < 0.01$). In **c**–**f,** the asterisk indicates a significant difference in photosynthetic rate, starch, soluble sugar, and NSC between CK and LSF group ($n = 36$, $P < 0.01$). The box spans from the first to the third quartile, with intermediate values marked as the black line in the middle of the box. In **k** and **l**, LSF, $GPP_{current}$, and start of growing season in the current year ($SOS_{current}$) were incorporated into the SEM to explore the direct (arrows from each factor directly pointing to the SOS_{next}) or indirect (arrows from each factor firstly directly pointing to $GPP_{current}$ then to the SOS_{next}) effects of factors on spring phenology in the next year. The calculated *P* values based on two-sided test and other statistics were listed in Supplementary Table 4. In **m–p,** the error bars indicate standard errors of the mean (n = 10698).

Fig. 4 | Projected effect of late spring frost (LSF) on start of growing season (SOS) in the next year at the end of this century (2080-2100) across different models under four climatic scenarios. a–d, Spatial distribution of mean ΔSOS when LSF occurred from the Coupled Model Intercomparison Project Phase 6 (CMIP6) models under SSP1-2.6 (**a**), SSP2-4.5 (**b**), SSP3-7.0 (**c**), and SSP5-8.5 (**d**). **e–h**, Spatial distribution of mean ΔSOS when LSF occurred from the sequential model (SM) with GPP effects under SSP1-2.6 (**e**), SSP2-4.5 (**f**), SSP3-7.0 (**g**), and SSP5-8.5 (**h**). **i–l**, Changes in ΔSOS across different models under SSP1-2.6 (**i**), SSP2-4.5 (**j**), SSP3-7.0 (**k**), and SSP5-8.5 (**l**). In **a–l**, ΔSOS indicates difference in SOS for each consecutive two-year period at each pixel. Y-CMIP indicates LSF occurred using CMIP6 models, Y-SM indicates LSF occurred using modified SM, and N indicates LSF did not occur using CMIP6 models. The SOS dates from 2080 to 2010 were extracted by daily gross primary productivity (GPP) dataset from CMIP6 models. In **i–l**, different letters indicate significant differences among different models based on Tukey's HSD test (P < 0.01). The detailed statistics were listed in Supplementary Table 6. The box spans from the first to the third quartile, with intermediate values marked as the black line in the middle of the box.

Fig. 5 | A schematic diagram of the interactions between late spring frost (LSF), photosynthetic carbon uptake, and spring phenology. The LSF in the current year could delay spring phenology in the next year by reducing photosynthetic carbon uptake in the current year. This LSF-induced delayed spring phenology in the next year can further reduce photosynthetic carbon uptake in the next year through feedback control.

Reference

1. Montgomery, R. A., Rice, K. E., Stefanski, A., Rich, R. L. & Reich, P. B. Phenological responses of temperate and boreal trees to warming depend on ambient spring temperatures, leaf habit, and geographic range. *Proceedings of the National Academy of Sciences* **117**, 10397–10405 (2020).
2. Thackeray, S. J. *et al.* Phenological sensitivity to climate across taxa and trophic levels. *Nature* **535**, 241–245 (2016).
3. Hufkens, K. *et al.* Ecological impacts of a widespread frost event following early spring leaf-out. *Global Change Biology* **18**, 2365–2377 (2012).
4. Reichstein, M. *et al.* Climate extremes and the carbon cycle. *Nature* **500**, 287–295 (2013).
5. Vitasse, Y., Lenz, A., Hoch, G. & Körner, C. Earlier leaf-out rather than difference in freezing resistance puts juvenile trees at greater risk of damage than adult trees. *Journal of Ecology* **102**, 981–988 (2014).
6. Weiser, C. J. Cold Resistance and Injury in Woody Plants. *Science* **169**, 1269–1278 (1970).
7. Lenz, A., Hoch, G., Vitasse, Y. & Körner, C. European deciduous trees exhibit similar safety margins against damage by spring freeze events along elevational gradients. *New Phytologist* **200**, 1166–1175 (2013).
8. Vitra, A., Lenz, A. & Vitasse, Y. Frost hardening and dehardening potential in temperate trees from winter to budburst. *New Phytologist* **216**, 113–123 (2017).
9. Augspurger, C. K. Reconstructing patterns of temperature, phenology, and frost damage over 124 years: Spring damage risk is increasing. *Ecology* **94**, 41–50 (2013).
10. Ma, Q., Huang, J.-G., Hänninen, H. & Berninger, F. Divergent trends in the risk of spring frost damage to trees in Europe with recent warming. *Global Change Biology* **25**, 351–360 (2019).
11. Piao, S. *et al.* Leaf onset in the northern hemisphere triggered by daytime temperature. *Nat Commun* **6**, 6911 (2015).
12. Wang, J. *et al.* Contrasting temporal variations in responses of leaf unfolding to daytime and nighttime warming. *Global Change Biology* **27**, 5084–5093 (2021).
13. Guo, J. *et al.* Meta-analytic and experimental evidence that warmer climate leads to shift from advanced to delayed spring phenology. *Agricultural and Forest Meteorology* **342**, 109721 (2023).
14. Keenan, T. F. *et al.* Net carbon uptake has increased through warming-induced changes in temperate forest phenology. *Nature Clim Change* **4**, 598–604 (2014).
15. Piao, S. *et al.* Plant phenology and global climate change: Current progresses and challenges. *Global Change Biology* **25**, 1922–1940 (2019).
16. Zohner, C. M. *et al.* Late-spring frost risk between 1959 and 2017 decreased in North America but increased in Europe and Asia. *Proceedings of the National Academy of Sciences* **117**, 12192–12200 (2020).
17. Huang, J.-G. *et al.* Intra-annual wood formation of subtropical Chinese red pine shows better

growth in dry season than wet season. *Tree Physiology* **38**, 1225–1236 (2018).

18. Knowles, J. F. *et al.* Montane forest productivity across a semiarid climatic gradient. *Global Change Biology* **26**, 6945–6958 (2020).
19. Amico Roxas, A., Orozco, J., Guzmán-Delgado, P. & Zwieniecki, M. A. Spring phenology is affected by fall non-structural carbohydrate concentration and winter sugar redistribution in three Mediterranean nut tree species. *Tree Physiology* **41**, 1425–1438 (2021).
20. Palacio, S., Maestro, M. & Montserrat-Martí, G. Seasonal dynamics of non-structural carbohydrates in two species of mediterranean sub-shrubs with different leaf phenology. *Environmental and Experimental Botany* **59**, 34–42 (2007).
21. Sperling, O., Earles, J. M., Secchi, F., Godfrey, J. & Zwieniecki, M. A. Frost Induces Respiration and Accelerates Carbon Depletion in Trees. *PLOS ONE* **10**, e0144124 (2015).
22. Davidson, A. M., Le, S. T., Cooper, K. B., Lange, E. & Zwieniecki, M. A. No time to rest: seasonal dynamics of non-structural carbohydrates in twigs of three Mediterranean tree species suggest year-round activity. *Sci Rep* **11**, 5181 (2021).
23. Löiez, S. & Piper, F. I. Phenology explains different storage remobilization in two congeneric temperate tree species with contrasting leaf habit. *Tree Physiology* **42**, 501–512 (2022).
24. Gu, L. *et al.* The 2007 Eastern US Spring Freeze: Increased Cold Damage in a Warming World? *BioScience* **58**, 253–262 (2008).
25. Svystun, T., Lundströmer, J., Berlin, M., Westin, J. & Jönsson, A. M. Model analysis of temperature impact on the Norway spruce provenance specific bud burst and associated risk of frost damage. *Forest Ecology and Management* **493**, 119252 (2021).
26. Jönsson, A. M., Linderson, M.-L., Stjernquist, I., Schlyter, P. & Bärring, L. Climate change and the effect of temperature backlashes causing frost damage in *Picea abies*. *Global and Planetary Change* **44**, 195–207 (2004).
27. Lang, G. A. Dormancy: A New Universal Terminology. *HortScience* **22**, 817–820 (1987).
28. Fu, Y. H. *et al.* Declining global warming effects on the phenology of spring leaf unfolding. *Nature* **526**, 104–107 (2015).
29. Strimbeck, G. R., Kjellsen, T. D., Schaberg, P. G. & Murakami, P. F. Dynamics of low-temperature acclimation in temperate and boreal conifer foliage in a mild winter climate. *Tree Physiology* **28**, 1365–1374 (2008).
30. Gaumont-Guay, D., Margolis, H. A., Bigras, F. J. & Raulier, F. Characterizing the frost sensitivity of black spruce photosynthesis during cold acclimation. *Tree Physiology* **23**, 301–311 (2003).
31. Lee, J. W., Lee, S. H., Han, J. W. & Kim, G. H. Early Light-Inducible Protein (ELIP) Can Enhance Resistance to Cold-Induced Photooxidative Stress in Chlamydomonas reinhardtii. *Frontiers in Physiology* **11**, (2020).
32. D'Andrea, E. *et al.* Winter's bite: beech trees survive complete defoliation due to spring late-frost damage by mobilizing old C reserves. *New Phytologist* **224**, 625–631 (2019).

33. D'Andrea, E. *et al.* Unravelling resilience mechanisms in forests: role of non-structural carbohydrates in responding to extreme weather events. *Tree Physiology* **41**, 1808–1818 (2021).
34. Masson-Delmotte, V. P. *et al. IPCC, 2021: Summary for Policymakers. In: Climate Change 2021: The Physical Science Basis. Contribution of Working Group I to the Sixth Assessment Report of the Intergovernmental Panel on Climate Change*. https://researchspace.csir.co.za/dspace/handle/10204/12710 (2021).
35. Lambert, M. S. A. *et al.* Inclusion of a cold hardening scheme to represent frost tolerance is essential to model realistic plant hydraulics in the Arctic–boreal zone in CLM5.0-FATES-Hydro. *Geoscientific Model Development* **15**, 8809–8829 (2022).
36. Lambert, M. S. A. *et al.* Integration of a Frost Mortality Scheme Into the Demographic Vegetation Model FATES. *Journal of Advances in Modeling Earth Systems* **15**, e2022MS003333 (2023).
37. Meyer, B. F. *et al.* Frost matters: incorporating late-spring frost into a dynamic vegetation model regulates regional productivity dynamics in European beech forests. *Biogeosciences* **21**, 1355–1370 (2024).
38. Fu, Y. *et al.* Progress in plant phenology modeling under global climate change. *Sci. China Earth Sci.* **63**, 1237–1247 (2020).
39. Brodribb, T. J., Pittermann, J. & Coomes, D. A. Elegance versus Speed: Examining the Competition between Conifer and Angiosperm Trees. *International Journal of Plant Sciences* **173**, 673–694 (2012).
40. Fisichelli, N., Vor, T. & Ammer, C. Broadleaf seedling responses to warmer temperatures "chilled" by late frost that favors conifers. *Eur J Forest Res* **133**, 587–596 (2014).
41. Vitasse, Y. *et al.* Contrasting resistance and resilience to extreme drought and late spring frost in five major European tree species. *Global Change Biology* **25**, 3781–3792 (2019).
42. Chen, L. *et al.* Long-term changes in the impacts of global warming on leaf phenology of four temperate tree species. *Global Change Biology* **25**, 997–1004 (2019).
43. Körner, C. & Basler, D. Phenology Under Global Warming. *Science* **327**, 1461–1462 (2010).

Methods

Phenological data

Ground-based phenology network

The start of growing season (SOS) was obtained from the Pan European Phenology Network (PEP725), USA National Phenology Network (USA-NPN), China Phenological Observation Network (CPON), and Russian 'Chronicles of Nature' Network (RCNN). The PEP725 contains *in situ* phenological observations of many temperate species across central Europe since 1868[44], The USA-NPN includes plant phenological records of 400 species at 3000 sites in conterminous United States[45]. The CPON involves phenological data at 44 sites in China starting in 1963[46]. The RCNN has 506,186 phenological observations at 471 sites in Russian Federation, Ukraine, Uzbekistan, Belarus and Kyrgyzstan[47]. Due to the different definitions of spring phenological events for each ground-based network, we screened the phenological observations of all four ground phenological network according to distinct criteria (Supplementary Note 1).

PhenoCam network

PhenoCam network (https://phenocam.sr.unh.edu/) is a cooperative continental-scale repository. The network uses digital phenocamera imagery to track the timing of phenological transition from 2000 to 2018 in North America and around the world[48]. In the PhenoCam network, the 50th, 75th and 90th percentile of the Green Chromatic Coordinate (G_{CC}) were calculated to extract the date of greenness rising and falling based on the following formula:

$$G_{CC} = \frac{G_{DN}}{R_{DN} + G_{DN} + B_{DN}} \tag{1}$$

where R_{DN}, G_{DN} and B_{DN} denotes the average digital numbers (DN) of red, green and blue color channels across the region of interest (ROI), respectively.

We used the 50% threshold of 90th percentile G_{CC} as spring leaf-out[49]. We removed outliers more than 2.5 times of MAD[50]. We obtained three forest types: evergreen needleleaf forests (ENF), deciduous needleleaf forests (DNF), and deciduous broadleaf forests (DBF). Ultimately, we selected 529 records at 67 sites with at least five years of observations between 2000 and 2018.

GIMMS NDVI3g phenological product

Over recent decades, satellite remote sensing data have been widely used to detect long-term and large-scale plant phenological events[51]. We derived SOS metrics from the GIMMS NDVI3g dataset (http://ecocast.arc.nasa.gov) produced by Advanced Very High Resolution Radiometer (AVHRR) instruments between 1982 and 2014 at 0.08° spatial resolution and 15-day temporal resolution[52]. We excluded non-vegetated areas with annual average NDVI < 0.1 to reduce bias.

We used Savitzky-Golay filter to smooth the time series and minimize the noise of atmospheric interference and satellite sensor before the estimation of spring phenology[53]. We then applied a double logistic function (Eq. 2) to fit annual NDVI time series curve, and calculated the second-order derivative of the fitted curve[51]. The SOS was defined as the date when the rate of change in curvature reached its first local maximum value in the first half year.

$$y(t) = a + b\left(\frac{1}{1+e^{c(t-d)}} + \frac{1}{1+e^{e(t-f)}}\right) \tag{2}$$

where b, c, d, and f are parameters of logistic function, and a is the initial background NDVI value, $a + b$ denotes the maximum NDVI value, t is time in days, and $y(t)$ is the NDVI value at time t.

MODIS phenological product

The MODIS land surface phenology product (MCD12Q2 V6) was downloaded from the Land Processes Distributed Active Archive Center (LPDAAC) (https://lpdaac.usgs.gov/)[54]. The MCD12Q2 product provides annual characteristics of vegetation phenology at a spatial resolution of 500 m between 2001 and 2019 on a global scale. The phenological metrics were derived from time series of the two-band enhanced vegetation index (EVI2), which is calculated from MODIS nadir BRDF adjusted surface reflectance (NBAR-EVI2). We selected the "Greenup" phase to define SOS and to represent spring leaf-out. The SOS was defined as the date when the EVI2 first crossed 15% of the segment EVI2 amplitude.

Future phenological data

Due to the absence of future NDVI and EVI data, we extracted phenological metrics using daily gross primary productivity (GPP) and leaf area index (LAI) dataset to predict future phenology shifts at the end of this century (2080-2100) under four climatic scenarios (SSP1-2.6, SSP2-4.5, SSP3-7.0 and SSP5-8.5). GPP and LAI data for the period 2080-2100 was obtained from the NorESM2-MM model at 1° spatial resolution, which is a component of the Coupled Model Intercomparison Project Phase 6 (CMIP6, https://esgf-node.llnl.gov/projects/esgf-llnl/). We first used Savitzky-Golay filter to smooth the time series and exclude abnormal daily GPP (or LAI) values before estimating spring phenology[53]. We then applied a double logistic function (Eq. 2) to fit annual GPP (or LAI) time series and extracted SOS[51], which is defined as the date when the rate of change in curvature reached its first local maximum value in the first half year.

Gross primary productivity and net primary productivity data

The annual GPP and net primary productivity (NPP) datasets between 1982 and 2018 were obtained from the global land surface satellite (GLASS) product (http://www.glass.umd.edu/index.html) at 0.05° spatial resolution[55].

Remote-sensing vegetation indices

We utilized two complementary remote-sensing vegetation indices, the Normalized Difference Vegetation Index (NDVI) and the Enhanced Vegetation Index (EVI), to quantify the impact of late spring frost (LSF) on tree growth. NDVI and EVI data from 2001 to 2019 were derived from Terra MODIS vegetation indices products (MOD13A1) at 500 m spatial resolution and 16-day temporal resolution.

Tree-ring width data

We also used raw tree-ring width (TRW) and basal area increment (BAI) to examine the effect of LSF on tree growth and productivity[56]. TRW data were obtained from the International Tree-Ring Data Bank (ITRDB) database and ref.[57]. In total, we remained 35,716 TRW records of 66 tree species at 1855 sites with at least 15 years of observations during 1982-2014 in the Northern Hemisphere. BAI, a two-dimensional measure, provides a more accurate quantification of wood production compared to TRW[58]. Due to the lack of field-measured diameters in the ITRDB database, we calculated diameters from the sum of annual raw TRWs in accordance with previous studies[59,60]. The BAI of each tree-ring core was calculated using Eq. 3.

$$\mathrm{BAI} = \pi\ (\mathrm{R}_t^2 - \mathrm{R}_{t\text{-}1}^2) \quad (3)$$

where R denotes the radius, and *t* represents the year of tree ring formation.

MODIS land cover product

The MODIS land cover product (MCD12Q1) with the International Geosphere-Biosphere Programme (IGBP) classification scheme at 500m spatial resolution was used to define the vegetation types[61]. The IGBP classification scheme includes 17 land cover types. We excluded non-forest vegetation types and reclassified the original forest types into the needleleaf forests, broadleaf forests, mixed forests, and woody savannas.

Global climate zones product

The Global ecological zone (GEZ) of the Forest Resources Assessment with a spatial resolution of 0.05° was used to define the climate zones[62]. We only kept areas outside the tropics (latitudes >30 °N) that have clear seasonal phenological cycles, and classified forest biomes into subtropical forests, temperate forests, and boreal forests based on GEZ 2010 map.

Climate data

Gridded daily minimum temperature during 1950-2013 in Europe were obtained from the database E-OBS (http://www.ecad.eu/) with 0.25° spatial resolution to match the PEP725 phenological dataset. We also used global daily minimum and average temperatures during 1950-2020 from the CRU JRA v2.2 dataset at 0.5° spatial resolution to match other phenological datasets. Monthly Standardized Precipitation-Evapotranspiration Index (SPEI) between 1982 and 2019 were extracted from the global 0.5° gridded SPEI dataset (SPEIbase v.2.9) (http://hdl.handle.net/10261/332007). Monthly Palmer Drought Severity Index (PDSI) data from 2001 to 2019 were derived from TerraClimate dataset at 4 km spatial resolution[63]. Future daily minimum and average temperatures during 2080-2100 were obtained from the CMIP6 model (NorESM2-MM) under four climatic scenarios (SSP1-2.6, SSP2-4.5, SSP3-7.0 and SSP5-8.5) with 1° spatial resolution. To address the difference in the spatial resolutions of various remote sensing datasets, all satellite remote sensing datasets were resampled to 0.25° spatial resolution. Then, the bilinear interpolation method was used to extract climate data for each site or pixel using the “raster” package[64] in R[65].

Spring phenology models

We used four process-based phenology models to simulate and predict spring phenology, including one-phase growing degree days model (GDD)[66], spring warming model (SW)[67], two-phase sequential model (SM)[68] and parallel model (PM)[69] (Supplementary Note 2).

Statistical analysis

We first investigated the carry-over effect of LSF on spring phenology using five ground-based phenological and PhenoCam networks, and remotely sensed data from 1950 to 2020 in the Northern Hemisphere. To clarify the frost-induced changes in spring phenology, we then examined the effect of LSF on photosynthetic productivity using remote sensing data (i.e., GPP and NPP) and frost-controlled growth chamber experiments. To test the robustness of our results, we also quantified the impact of LSF on tree growth and productivity using remote-sensing vegetation indices (i.e., NDVI and EVI), and tree-ring width (i.e., TRW and BAI) in the Northern Hemisphere. Considering that GPP and NPP data are more closely connected to the growth of leaves and canopies compared to tree-ring width records, GPP and NPP data were further utilized to examine the effect of LSF on photosynthetic productivity in the next year. Lastly, we projected the effect of LSF on spring phenology based on CMIP6 models and modified SM under four future climatic scenarios (Extended Data Fig. 5).

Effect of LSF on spring phenology

Previous studies showed that spring temperatures fall below −2°C may significantly affect the growth and survival of trees[5,10]. Here, we defined the LSF event as the last frost event (i.e., when daily minimum temperature falls below −2°C) that occurred between the period after SOS and before 15 July[7].

To examine the carry-over effect of LSF on spring phenology in the next year, we calculated and compared the changes in SOS of the next year (SOS_{next}) at each site or pixel using multi-source observational data when LSF occurred or did not (ground phenological network, PhenoCam network, and satellite remote sensing products) across the Northern Hemisphere. To this end, we first calculated the difference in SOS (ΔSOS) for each consecutive two-year period according to Eq.4. Then, we identified whether LSF occurred at each site (pixel) in each year, and compared the difference of ΔSOS when LSF occurred or not.

$$\Delta \mathrm{SOS} = \mathrm{DOY}_{t+1} - \mathrm{DOY}_{t} \tag{4}$$

where the DOY_t is the timing of SOS in year t, and DOY_{t+1} is the timing of SOS in the next year t+1. One-way analysis of variance (ANOVA) was used to test the difference in the ΔSOS when LSF occurred or not for each phenological dataset. Using linear mixed model, we further examined the overall effect of LSF on SOS_{next} by pooling all the ground-based phenological datasets for a global test. In the model, the response variable was ΔSOS, the fixed effect was the occurrence of LSF, with random intercepts among sites and species.

In order to eliminate the influence of low preseason temperatures on spring phenology, we categorized preseasons into either cold or warm based on whether the mean minimum temperature during winter (November to January), spring (February to April), and the combined winter and spring months (November to April) of the specific year at the particular site fell below or above their long-term averages from 1982 to 2018, respectively. We employed one-way ANOVA to assess the variation in ΔSOS when LSF occurred or did not occur during cold and warm preseasons. To test the robustness of our results, we further examined the effects of both spring temperature and LSF on timing of leaf-out using a linear mixed model. In this model, the response variable is ΔSOS, the predictors are the occurrence of LSF (a categorical variable with two levels: occurrence and non-occurrence) and the difference in spring temperature, with species and sites are set as random effects. To address the species-specific frost response, we divided the tree species into early-leafing species and late-leafing species based on the mean SOS date of all species in each ground-based phenological dataset. One-way ANOVA was used to test the difference in the ΔSOS between early- and late-leafing species, and between broadleaf and conifer species using ground-based phenological data, also among different forest types and climate zones using remote sensing and ground-based phenological datasets. We also set the minimum temperature threshold of LSF at 0°C, −2°C, and −4°C to examine and compare the carry-over effect of different levels of LSF on spring phenology in the next year in eight deciduous tree species based on the PEP725 dataset, the largest ground phenological network used in our study. To ensure the reliability of our findings, we further incorporated the temporal dimension of frost damage into the LSF definition. Specifically, we redefined LSF to be the period from one to eight weeks after SOS and prior to July 15th, employing a range of temperature thresholds (0ºC, −2ºC, and −4ºC) based on ground phenological networks. Using one-week smoothing window, we re-examined carry-over effect of LSF on spring phenology based on ground-based phenological data. The accumulation of thermal units prior to the LSF potentially increases the susceptibility of immature leaves to sub-zero temperatures. Using the smoothing window, we also calculated the accumulated Growing Degree Days (GDD) exceeding 0°C from January 1st to the occurrence of LSF for assessing the temporal change in LSF risk[16].

Estimates of the lethal temperature

Among all the ground-based phenological networks, the period of phenological records in the PEP725 spanned nearly six decades, and was distributed at more than 1000 sites. To ensure the robustness of results, the long-term and large-scale SOS records from the PEP725 network were selected to calculate the lethal temperature of 50% leaves (LT_{50}) to further clarify differences in SOS_{next} in response to LSF among tree species. The LT_{50} is commonly determined by electrolyte leakage tests or visual damage assessment in the field or in the laboratory[70,71]. We conducted an extensive literature search and compiled LT_{50} in as many tree species as possible in the PEP725 dataset. Since LT_{50} is greatly affected by the leaf development stage, we only retained LT_{50} measured in spring leaf-out[5,7]. Ultimately, we obtained determined LT_{50} values in five tree species. Also, we used a four-parameter logistic model with two fixed asymptotes and two free parameters to estimate the LT_{50} of all eight selected temperate species in the PEP725 dataset (Eq. 5)[72]. Specifically, we used two asymptotes to limit the estimate below −1°C, which corresponds to the highest LT_{50} of woody plants observed in temperate regions[73], and above −7.5°C, which is close to the lowest measured LT_{50} obtained from literature. To ensure reliability, we extracted the median dates of long-term and multi-site SOS for each species to estimate the LT_{50}.

$$\mathrm{LT}_{50} = \frac{a-b}{1+\exp\left[\left(c-x\right)/d\right]}+b \tag{5}$$

where *a* and *b* are fixed parameters, a = −7.5 and b = −1, c and d are free parameters (estimated c = 130, d = −10), and *x* is the predictor variable (median date of leaf unfolding for each species). We conducted a non-linear model fitted using the "nlme" package[74] in R[65]. Correlation analysis was used to examine the relationship between the measured and calculated LT_{50} values. Linear regression model was used to examine the relationship between the LT_{50} predicted by the model and ΔSOS for each species in the PEP725 dataset.

Effect of LSF on photosynthetic productivity

We first matched GLASS GPP (or NPP) data with GIMMS NDVI3g and MODIS phenological products. We then analyzed the changes in the GPP and NPP in the current year ($GPP_{current}$, $NPP_{current}$) when LSF occurred or did not occur for each pixel using remote sensing data. One-way ANOVA was used to test the difference in the $GPP_{current}$ (or $NPP_{current}$) when LSF occurred or not in the current year. We also confirmed the LSF damage utilizing long-term and large-scale remote-sensing vegetation indices (NDVI and EVI) and tree-ring data (TRW and BAI) in the Northern Hemisphere. We further used structural equation models (SEM) to examine the relationships between LSF, $GPP_{current}$ (or $NPP_{current}$) and SOS_{next} using remote sensing data. We constructed a conceptual model that includes both the direct and indirect effects of LSF in the current year on SOS_{next}. In the SEM model, we hypothesized that LSF in current year is likely to directly affect the SOS_{next}, indicated by the arrows from LSF directly point to the SOS_{next}, or indirectly affect SOS_{next} by altering the photosynthetic carbon assimilation, indicated by the arrows from LSF firstly directly point to $GPP_{current}$ (or $NPP_{current}$) then to the SOS_{next}. Incidentally, SOS in the current year ($SOS_{current}$) may directly alter carbon storage, and then affect SOS_{next}. Therefore, $SOS_{current}$ is also included in SEM as a direct and indirect factor in the model. The piecewise SEM was fit using the "piecewiseSEM" package[75] in R[65]. To eliminate the potential impact of drought on $GPP_{current}$, we conducted an analysis of $GPP_{current}$ changes concerning the occurrence or absence of summer droughts (between July and September) in the current year, utilizing both 6- and 12-month SPEI data as well as PDSI data. For our analysis, a summer drought event was defined as when the mean SPEI dropped below −2 or when the mean PDSI fell below −4 during the summer months. We employed one-way ANOVA to assess the disparity in $\Delta GPP_{current}$ between instances where LSF occurred or did not occur in the current year. Using a frost-controlled experiment with four tree species widely distributed in temperate and subtropical forests (Supplementary Note 3), we further investigated the effect of LSF on photosynthetic rate and nonstructural carbohydrates (NSC) of stem and leaves to understand the mechanisms underlying the relationship between LSF and photosynthetic productivity. We also calculated species-specific shifts in photosynthetic rate, starch, soluble sugar, and total NSC between the control (CK) and LSF groups. we employed one-way ANOVA to analyze the differences in photosynthetic rate, starch, soluble sugar, and total NSC between the CK and LSF treatment,

Feedback effect of spring phenology on photosynthetic productivity

To evaluate whether LSF have an effect on carbon uptake in the subsequent year, one-way ANOVA were used to examine the differences in the GPP (or NPP) of the subsequent year (GPP_{next}, NPP_{next}) when LSF occurred and did not. In order to decipher the interactions between LSF, SOS and GPP, we further calculated and compared the differences in the GPP_{next} and

NPP_{next} anomaly (ΔGPP_{next}, ΔNPP_{next}) relative to the long-term average when SOS_{next} was advanced or delayed compared to $SOS_{current}$ for each pixel. One-way ANOVA was used to test the difference in ΔGPP_{next} (or ΔNPP_{next}) when SOS_{next} was advanced and delayed.

Projected effect of LSF on spring phenology under future climatic scenarios

We similarly used daily minimum temperature (below −2°C) to define LSF during 2080-2100 from the CMIP6 models under four climatic scenarios. We then used daily GPP data to extract future phenological metrics, and examined the effect of LSF on spring phenology based on CMIP6 models under four future climatic scenarios. Due to the superior performance of the modified SM, with solely the adjusted forcing phase, in simulating spring phenology when considering frost-induced in photosynthetic productivity, the modified SM was further used to predict the potential effects of LSF on shifts in spring phenology under future climatic scenario. One-way ANOVA followed by Tukey's HSD test was used to test the difference in mean ΔSOS when LSF occurred or not for different climatic scenarios using modified SM and original CMIP6 models. To minimize the uncertainties arising from a single phenological data, we also performed the same analysis to investigate effect of LSF on spring phenology using daily LAI data from CMIP6 models under four future climatic scenarios. We further assessed the temporal change in the carry-over effect of LSF and its risk utilizing ground phenological networks.

All data analyses were conducted using R version 4.1.1[65].

Data availability

All ground-based and remote-sensing derived phenological data are freely available on the following websites: Pan European Phenology Network (PEP725), http://www.pep725.eu/; USA National Phenology Network (USA-NPN), https://www.usanpn.org/results/data; China Phenological Observation Network (CPON), http://www.cpon.ac.cn/; Russian 'Chronicles of Nature' Network (RCNN), https://doi.org/10.1038/s41597-020-0376-z; PhenoCam, https://phenocam.sr.unh.edu/; GIMMS NDVI3g phenological product, https://globalecology.unh.edu/; MODIS phenological product, https://lpdaac.usgs.gov/. Gross primary productivity and net primary productivity data are available at http://www.glass.umd.edu/index.html. Gridded daily minimum and average temperatures can be downloaded from E-OBS (http://www.ecad.eu/) and CRU JRA v2.2 dataset (https://catalogue.ceda.ac.uk/uuid/4bdf41fc10af4caaa489b14745c665a6). Future minimum and average temperatures, GPP, and leaf area index (LAI) data were from the CMIP6 models (https://esgf-node.llnl.gov/projects/esgf-llnl/). Standardized Precipitation-Evapotranspiration Index (SPEI) dataset (SPEIbase v.2.9) are available on http://hdl.handle.net/10261/332007. Palmer Drought Severity Index (PDSI) data are available at https://climate.northwestknowledge.net/TERRACLIMATE/. MODIS vegetation indices and land cover data are available at https://ladsweb.modaps.eosdis.nasa.gov/. Raw tree-ring width data were obtained from the International Tree-Ring Data Bank (ITRDB) (https://www1.ncdc.noaa.gov/pub/data/paleo/treering/). Global ecological zone (GEZ) map is available at https://www.fao.org/forest-resources-assessment/remote-sensing/global-ecological-zones-gez-mapping/en/.

Code availability

All data analyses and modeling were performed using R version 4.1.1. The codes used for the model simulations in this study are available at https://doi.org/10.6084/m9.figshare.25844587.v1[76].

Reference

44. Templ, B. *et al.* Pan European Phenological database (PEP725): a single point of access for European data. *Int J Biometeorol* **62**, 1109–1113 (2018).
45. Schwartz, M. D., Betancourt, J. L. & Weltzin, J. F. From Caprio's lilacs to the USA National Phenology Network. *Frontiers in Ecology and the Environment* **10**, 324–327 (2012).
46. Ge, Q., Wang, H., Rutishauser, T. & Dai, J. Phenological response to climate change in China: a meta-analysis. *Global Change Biology* **21**, 265–274 (2015).
47. Ovaskainen, O. *et al.* Chronicles of nature calendar, a long-term and large-scale multitaxon database on phenology. *Sci Data* **7**, 47 (2020).
48. Richardson, A. D. *et al.* Tracking vegetation phenology across diverse North American biomes using PhenoCam imagery. *Sci Data* **5**, 180028 (2018).
49. Klosterman, S. T. *et al.* Evaluating remote sensing of deciduous forest phenology at multiple spatial scales using PhenoCam imagery. *Biogeosciences* **11**, 4305–4320 (2014).
50. Leys, C., Ley, C., Klein, O., Bernard, P. & Licata, L. Detecting outliers: Do not use standard deviation around the mean, use absolute deviation around the median. *Journal of Experimental Social Psychology* **49**, 764–766 (2013).
51. Wang, X. *et al.* No trends in spring and autumn phenology during the global warming hiatus. *Nat Commun* **10**, 2389 (2019).
52. Pinzon, J. E. & Tucker, C. J. A Non-Stationary 1981–2012 AVHRR NDVI3g Time Series. *Remote Sensing* **6**, 6929–6960 (2014).
53. Wang, X. *et al.* Validation of MODIS-GPP product at 10 flux sites in northern China. *International Journal of Remote Sensing* **34**, 587–599 (2013).
54. Friedl, M., Gray, J. & Sulla-Menashe, D. MODIS/Terra+Aqua Land Cover Dynamics Yearly L3 Global 500m SIN Grid V061 [Data set]. *NASA EOSDIS Land Processes DAAC* (2022).
55. Zheng, Y. *et al.* Improved estimate of global gross primary production for reproducing its long-term variation, 1982–2017. *Earth System Science Data* **12**, 2725–2746 (2020).

56. Xu, K. *et al.* Tree-ring widths are good proxies of annual variation in forest productivity in temperate forests. *Sci Rep* **7**, 1945 (2017).
57. Martínez-Sancho, E. *et al.* The GenTree Dendroecological Collection, tree-ring and wood density data from seven tree species across Europe. *Sci Data* **7**, 1 (2020).
58. Biondi, F. & Qeadan, F. A Theory-Driven Approach to Tree-Ring Standardization: Defining the Biological Trend from Expected Basal Area Increment. *trre* **64**, 81–96 (2008).
59. D'Orangeville, L. *et al.* Beneficial effects of climate warming on boreal tree growth may be transitory. *Nat Commun* **9**, 3213 (2018).
60. Tao, W. *et al.* Daytime warming triggers tree growth decline in the Northern Hemisphere. *Global Change Biology* **28**, 4832–4844 (2022).
61. Friedl, M. & Sulla-Menashe, D. MODIS/Terra+Aqua Land Cover Type Yearly L3 Global 500m SIN Grid V061 [Data set]. *NASA EOSDIS Land Processes DAAC* (2022).
62. FAO. Global Forest Resources Assessment 2010. *FAO Forestry Paper 163* (2010).
63. Abatzoglou, J. T., Dobrowski, S. Z., Parks, S. A. & Hegewisch, K. C. TerraClimate, a high-resolution global dataset of monthly climate and climatic water balance from 1958–2015. *Sci Data* **5**, 170191 (2018).
64. Hijmans, R. J. Raster: Geographic Data Analysis and Modeling. *R package. Version 3.5-2.* (2021).
65. R Core Team. R: A language and environment for statistical computing. *R Foundation for Statistical Computing* (2021).
66. Krinner, G. *et al.* A dynamic global vegetation model for studies of the coupled atmosphere-biosphere system. *Global Biogeochemical Cycles* **19**, (2005).
67. Cannell, M. G. R. & Smith, R. I. Thermal Time, Chill Days and Prediction of Budburst in Picea sitchensis. *Journal of Applied Ecology* **20**, 951–963 (1983).
68. Kramer, K. Selecting a Model to Predict the Onset of Growth of Fagus sylvatica. *Journal of Applied Ecology* **31**, 172–181 (1994).
69. Landsberg, J. J. Apple Fruit Bud Development and Growth; Analysis and an Empirical Model. *Annals of Botany* **38**, 1013–1023 (1974).
70. Bigler, C. & Bugmann, H. Climate-induced shifts in leaf unfolding and frost risk of European trees and shrubs. *Sci Rep* **8**, 9865 (2018).
71. Lenz, A., Hoch, G., Körner, C. & Vitasse, Y. Convergence of leaf-out towards minimum risk of freezing damage in temperate trees. *Functional Ecology* **30**, 1480–1490 (2016).
72. Hofmann, M., Jager, M. & Bruelheide, H. Relationship between frost hardiness of adults and seedlings of different tree species. *iForest - Biogeosciences and Forestry* **7**, 282 (2014).
73. Bannister, P. Godley review: A touch of frost? Cold hardiness of plants in the southern hemisphere. *New Zealand Journal of Botany* **45**, 1–33 (2007).
74. Pinheiro, J. Package 'nlme'. *Linear and nonlinear mixed effects models, version 3.1* **3**, 336 (2017).

75. Lefcheck, J. S. piecewiseSEM: Piecewise structural equation modelling in r for ecology, evolution, and systematics. *Methods in Ecology and Evolution* **7**, 573–579 (2016).

76. Hua, H., Wang, J., & Guo, J. Model codes of late spring frost (LSF) (Version 1). *figshare* https://doi.org/10.6084/m9.figshare.25844587.v1 (2024).

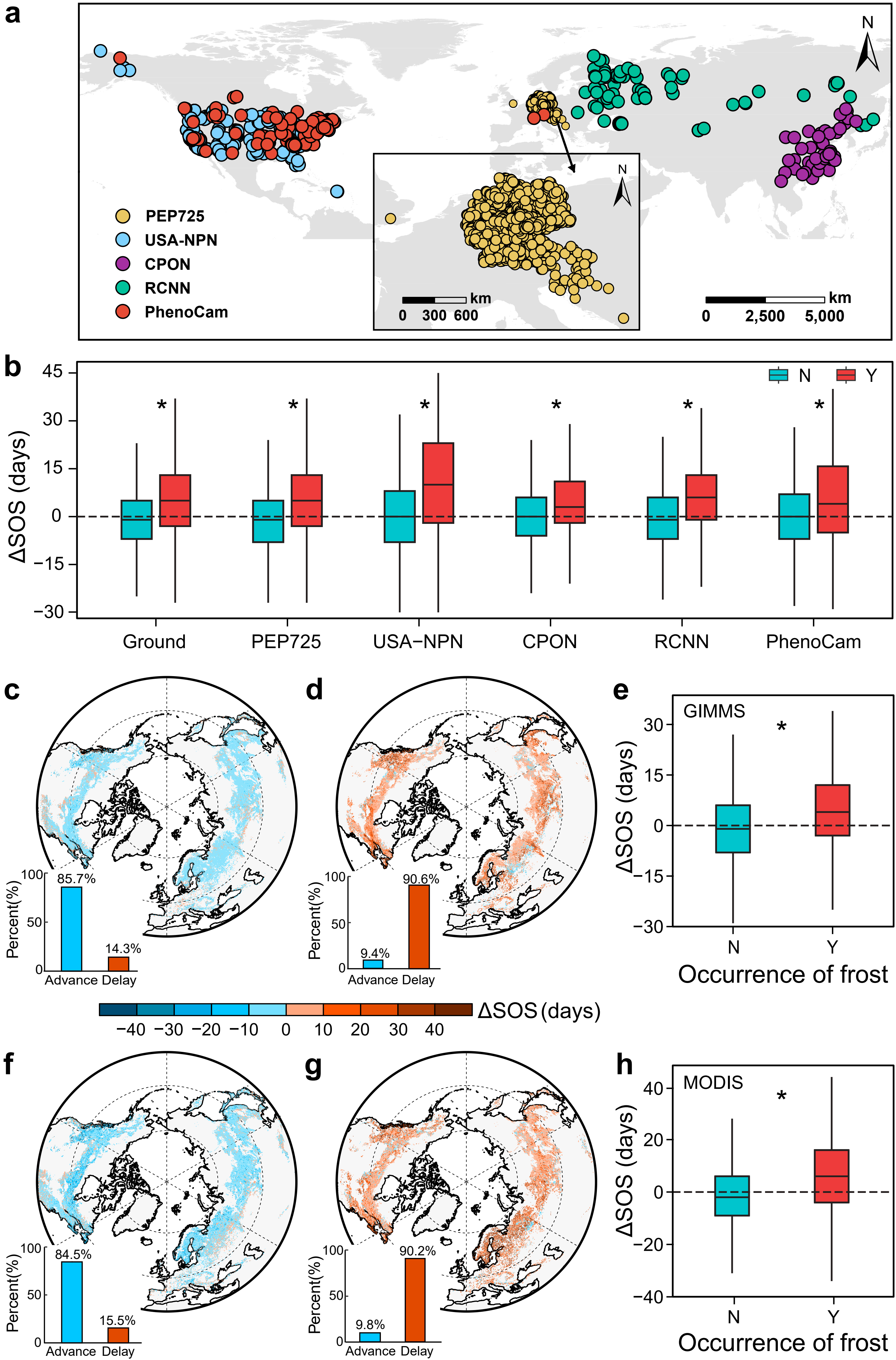
a
N
PEP725
USA-NPN
CPON
RCNN
PhenoCam
N
km
0 300 600
km
0 2,500 5,000
b
N Y
ΔSOS (days)
45
30
15
0
−15
−30
Ground
PEP725
USA−NPN
CPON
RCNN
PhenoCam
c
Percent(%)
85.7%
14.3%
Advance Delay
d
Percent(%)
9.4%
90.6%
Advance Delay
e
GIMMS
ΔSOS (days)
N
Y
Occurrence of frost
ΔSOS (days)
−40 −30 −20 −10 0 10 20 30 40
f
Percent(%)
84.5%
15.5%
Advance Delay
g
Percent(%)
9.8%
90.2%
Advance Delay
h
MODIS
ΔSOS (days)
N
Y
Occurrence of frost

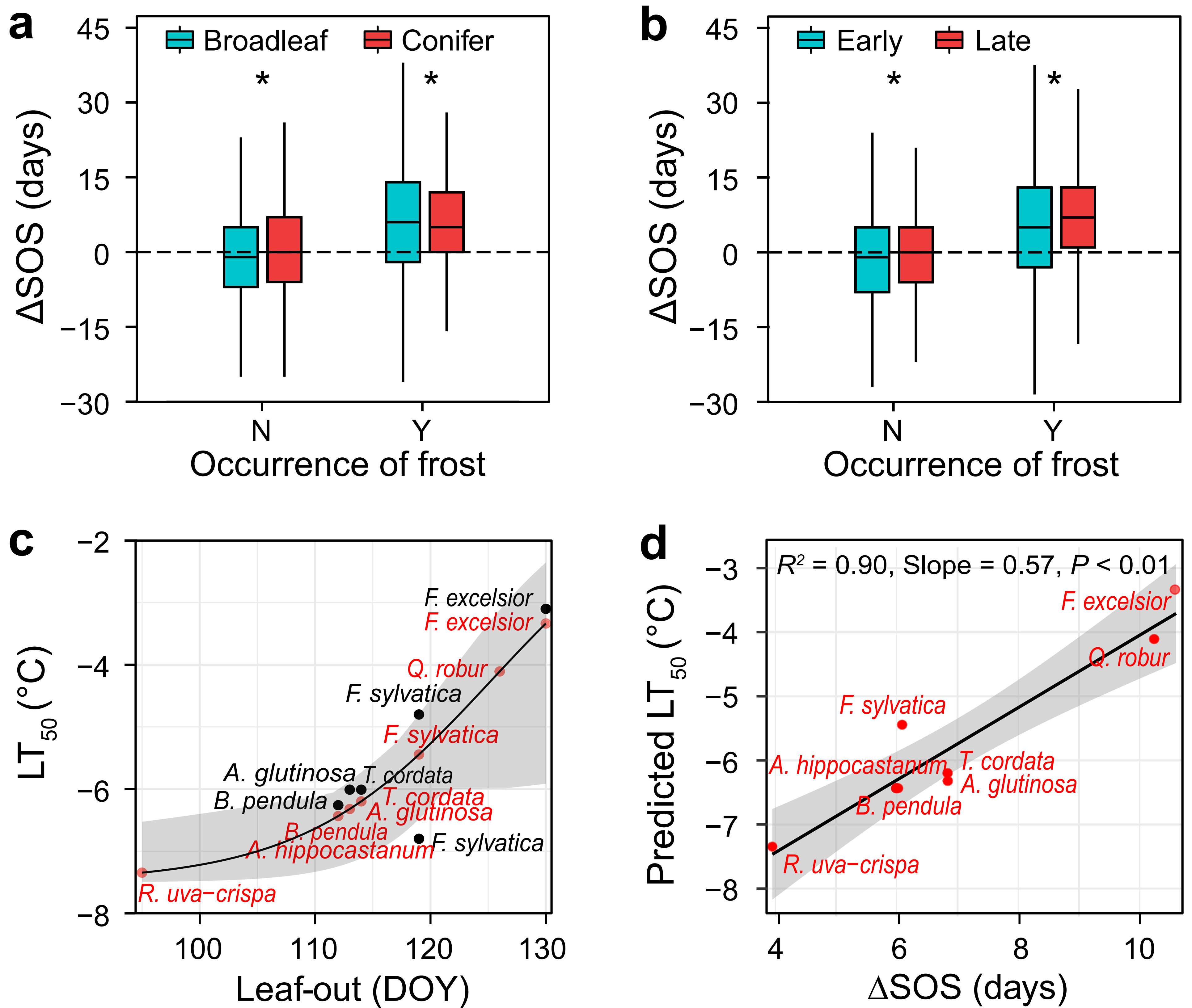
a
Broadleaf
Conifer
ΔSOS (days)
Occurrence of frost
N
Y
b
Early
Late
ΔSOS (days)
Occurrence of frost
c
LT50 (°C)
Leaf-out (DOY)
F. excelsior
Q. robur
F. sylvatica
A. glutinosa
T. cordata
B. pendula
A. hippocastanum
R. uva−crispa
d
R² = 0.90, Slope = 0.57, P < 0.01
Predicted LT50 (°C)
ΔSOS (days)

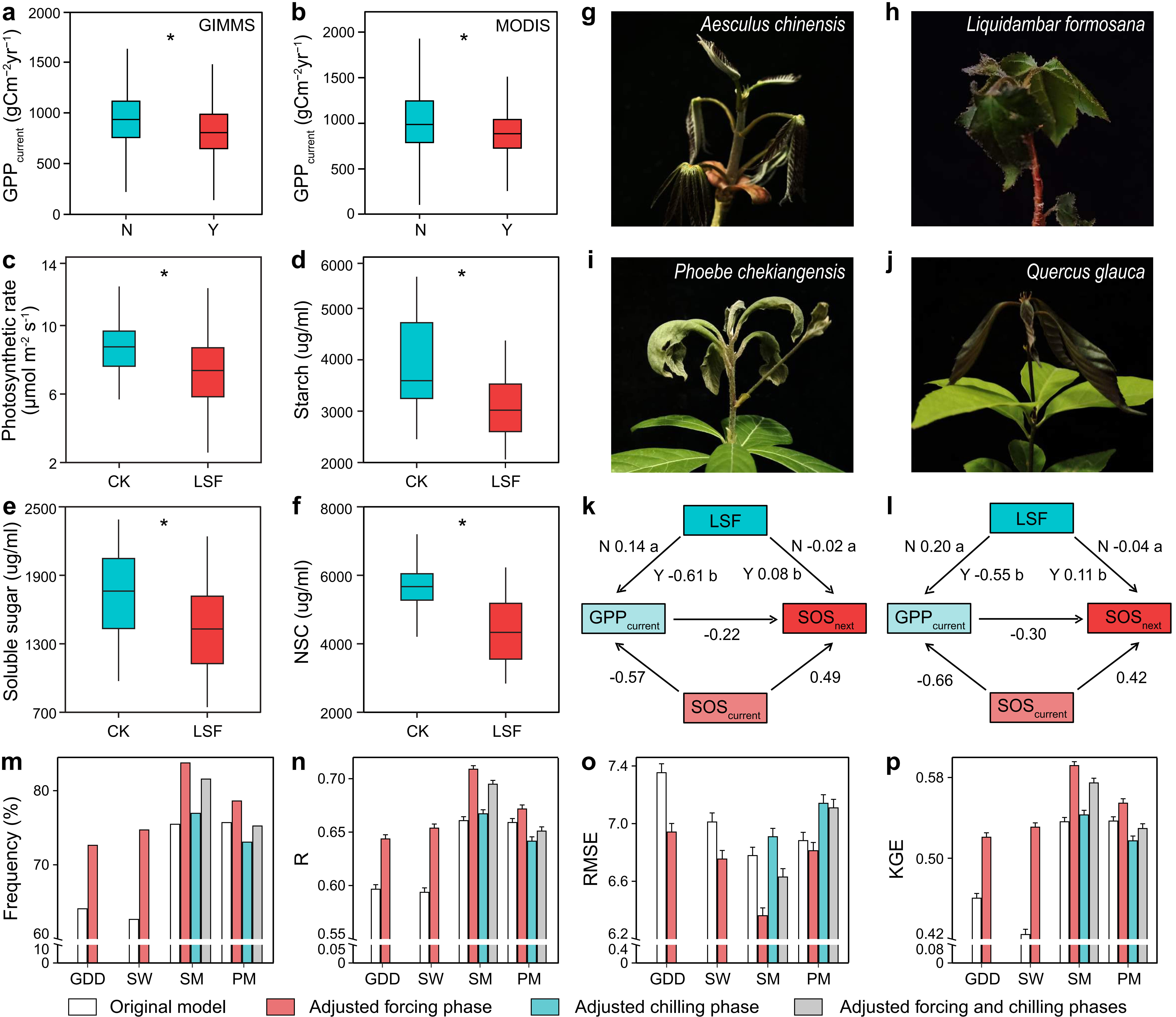

a
GIMMS
$GPP_{current}$ (gCm^{-2}yr^{-1})
N
Y
b
MODIS
c
Photosynthetic rate (μmol m^{-2} s^{-1})
CK
LSF
d
Starch (ug/ml)
e
Soluble sugar (ug/ml)
f
NSC (ug/ml)
g
Aesculus chinensis
h
Liquidambar formosana
i
Phoebe chekiangensis
j
Quercus glauca
k
LSF
N 0.14 a
Y -0.61 b
N -0.02 a
Y 0.08 b
$GPP_{current}$
SOS_{next}
-0.22
-0.57
0.49
$SOS_{current}$
l
N 0.20 a
Y -0.55 b
N -0.04 a
Y 0.11 b
-0.30
-0.66
0.42
m
Frequency (%)
n
R
o
RMSE
p
KGE
GDD
SW
SM
PM
Original model
Adjusted forcing phase
Adjusted chilling phase
Adjusted forcing and chilling phases

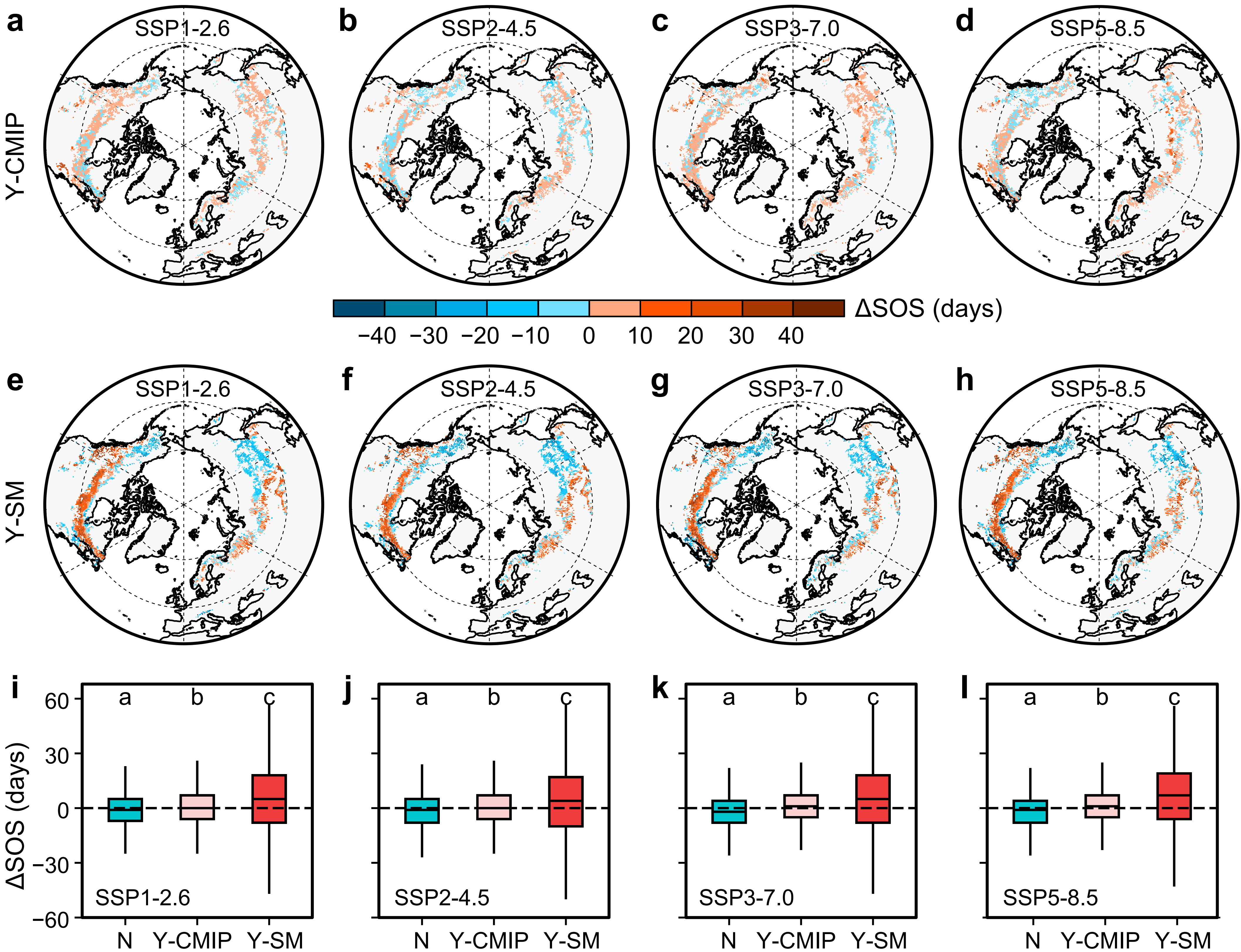

a
SSP1-2.6
b
SSP2-4.5
c
SSP3-7.0
d
SSP5-8.5
Y-CMIP
ΔSOS (days)
−40 −30 −20 −10 0 10 20 30 40
e
SSP1-2.6
f
SSP2-4.5
g
SSP3-7.0
h
SSP5-8.5
Y-SM
i
j
k
l
a b c
60
30
0
−30
−60
ΔSOS (days)
SSP1-2.6
SSP2-4.5
SSP3-7.0
SSP5-8.5
N Y-CMIP Y-SM

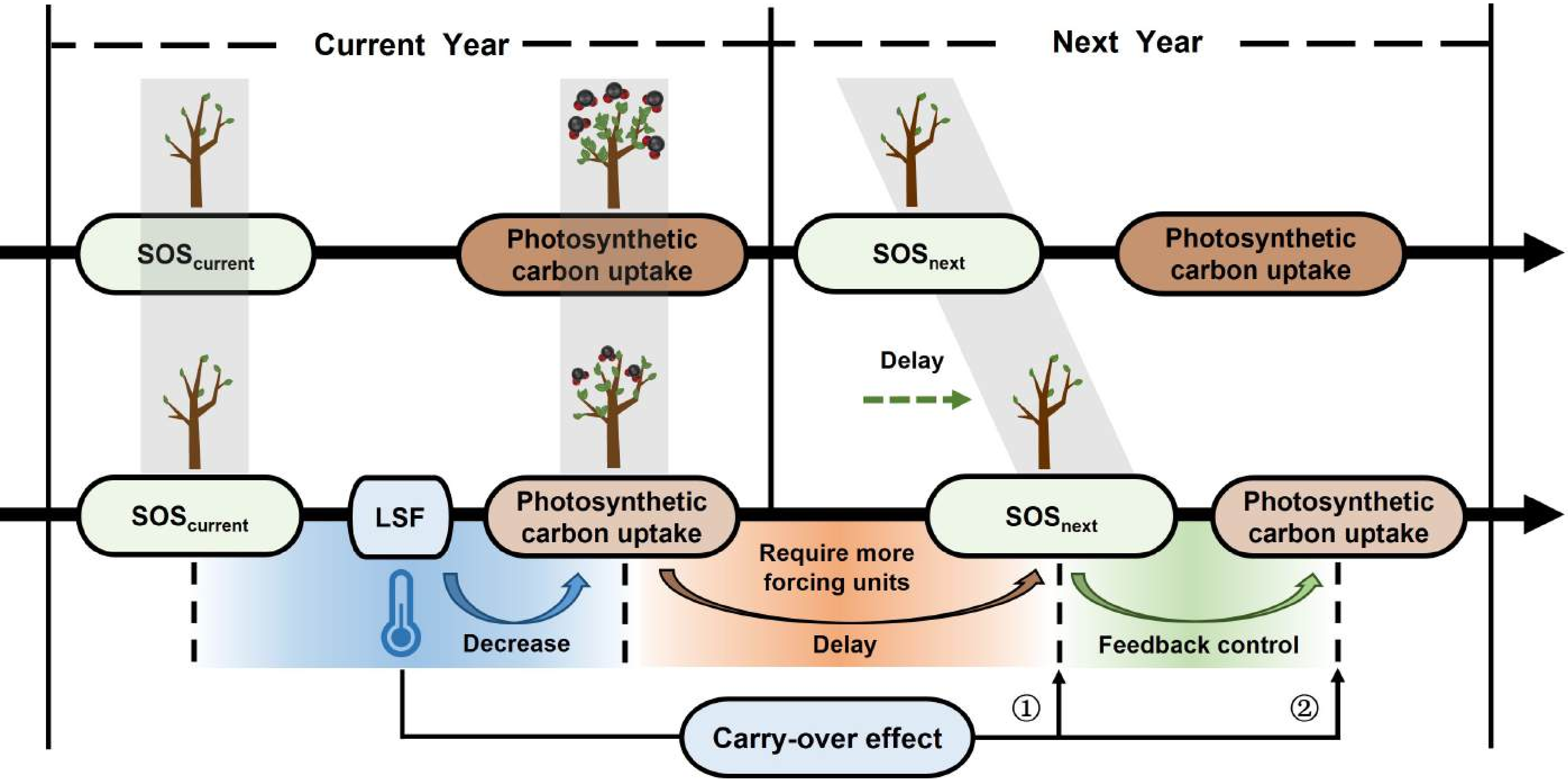
Current Year
Next Year
$SOS_{current}$
Photosynthetic carbon uptake
SOS_{next}
Photosynthetic carbon uptake
Delay
$SOS_{current}$
LSF
Photosynthetic carbon uptake
SOS_{next}
Photosynthetic carbon uptake
Require more forcing units
Decrease
Delay
Feedback control
①
②
Carry-over effect

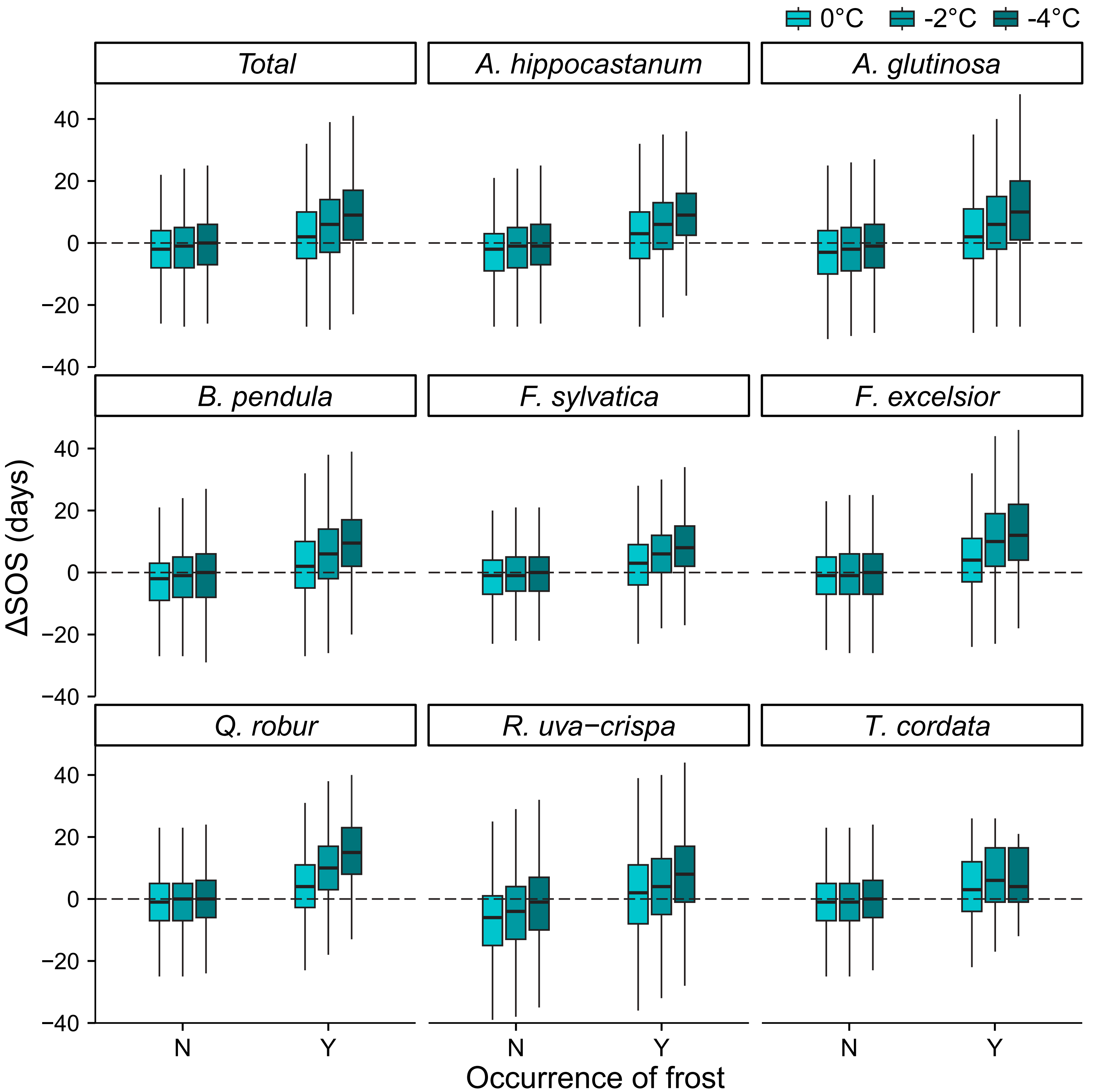
0°C
-2°C
-4°C
Total
A. hippocastanum
A. glutinosa
B. pendula
F. sylvatica
F. excelsior
Q. robur
R. uva−crispa
T. cordata
ΔSOS (days)
40
20
0
−20
−40
N
Y
Occurrence of frost

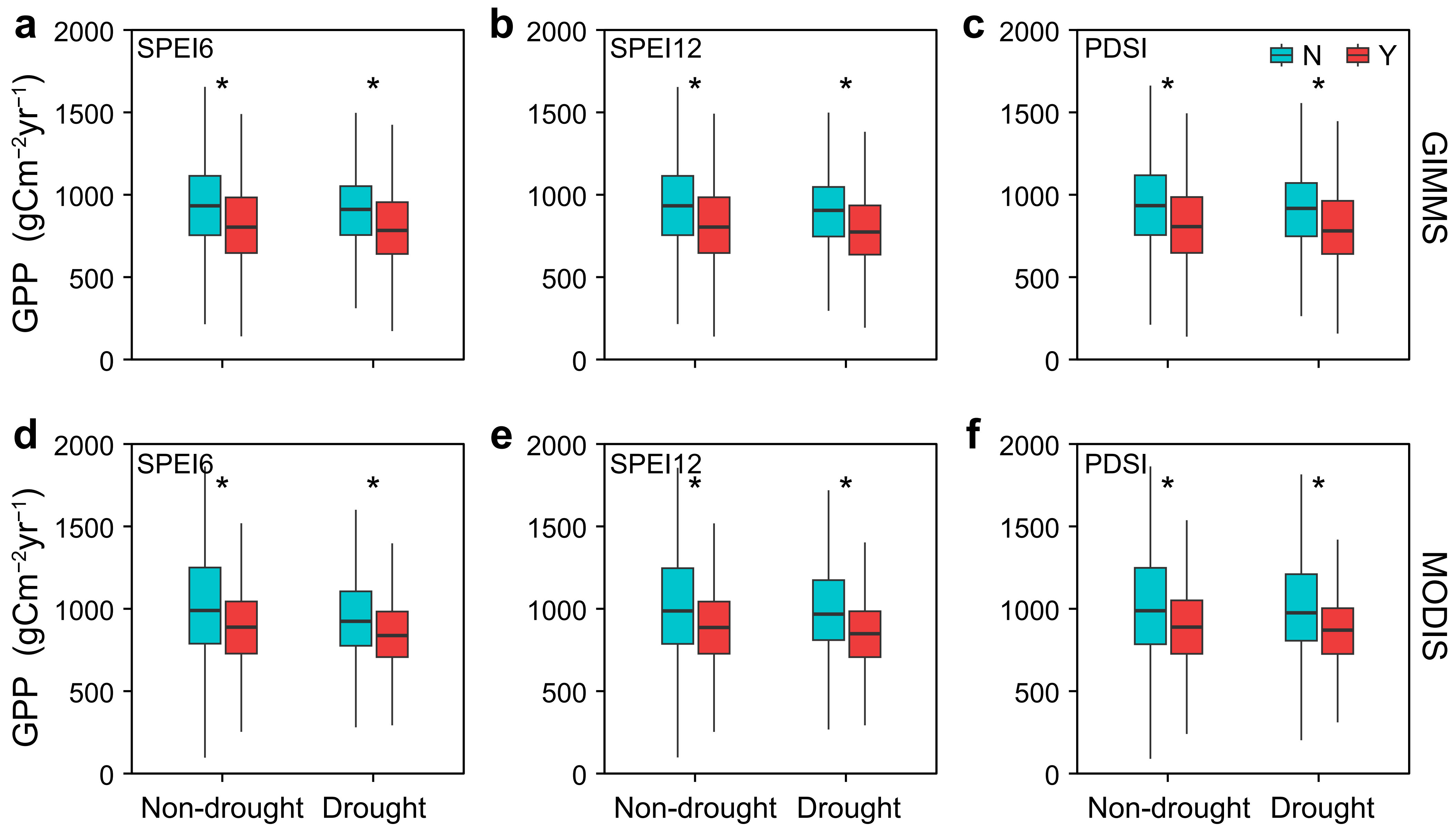

a
b
c
d
e
f
SPEI6
SPEI12
PDSI
N
Y
GPP (gCm^{-2}yr^{-1})
0
500
1000
1500
2000
Non-drought
Drought
GIMMS
MODIS

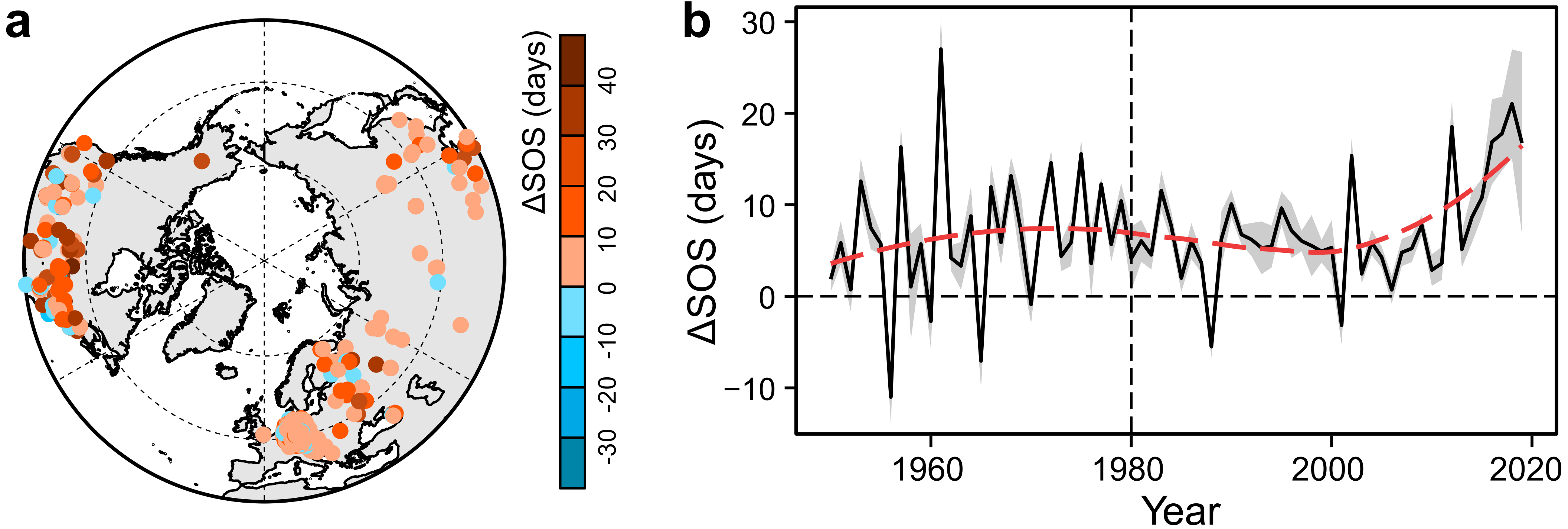

a
ΔSOS (days)
40
30
20
10
0
-10
-20
-30
b
30
20
10
0
−10
ΔSOS (days)
1960
1980
2000
2020
Year

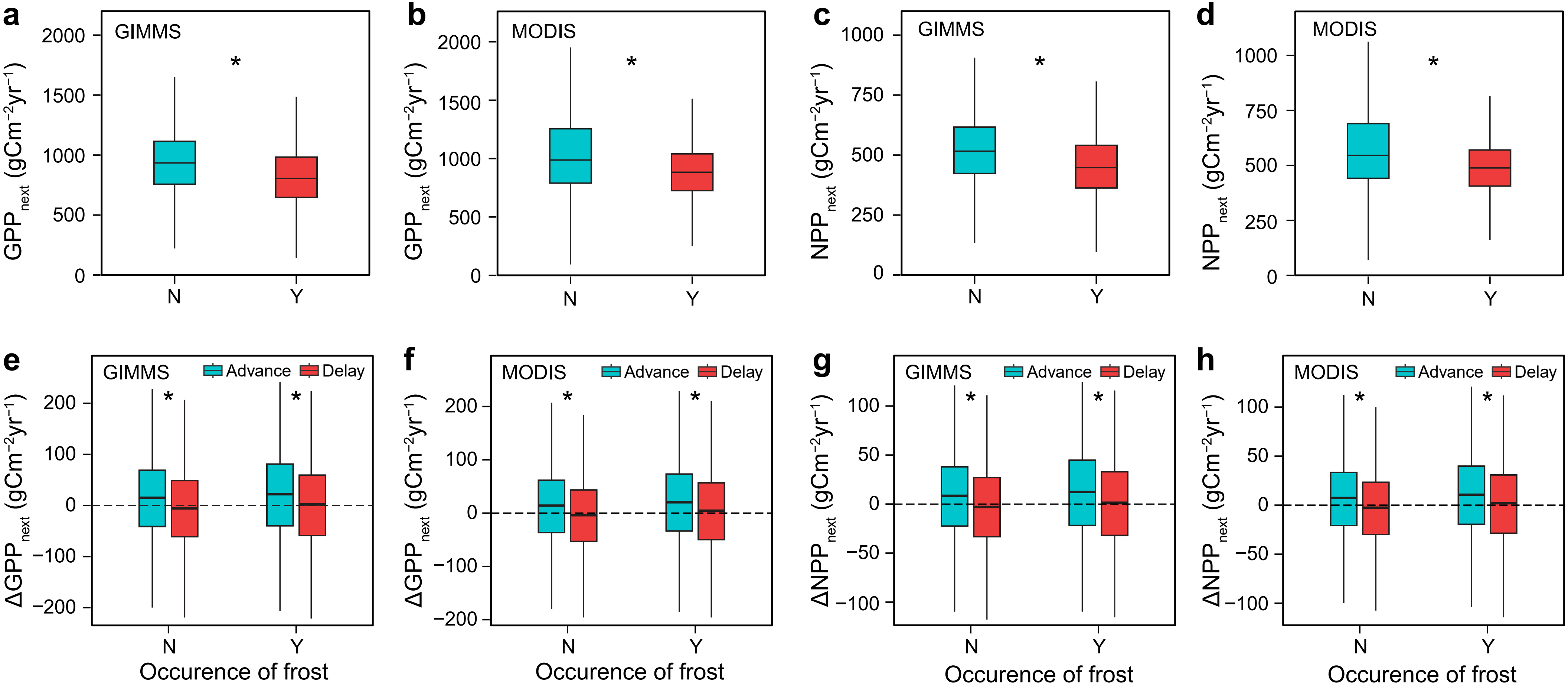
a
GIMMS
GPP$_{next}$ (gCm^{-2}yr^{-1})
b
MODIS
GPP$_{next}$ (gCm^{-2}yr^{-1})
c
GIMMS
NPP$_{next}$ (gCm^{-2}yr^{-1})
d
MODIS
NPP$_{next}$ (gCm^{-2}yr^{-1})
N
Y
e
GIMMS
Advance
Delay
ΔGPP$_{next}$ (gCm^{-2}yr^{-1})
f
MODIS
ΔGPP$_{next}$ (gCm^{-2}yr^{-1})
g
GIMMS
ΔNPP$_{next}$ (gCm^{-2}yr^{-1})
h
MODIS
ΔNPP$_{next}$ (gCm^{-2}yr^{-1})
Occurence of frost

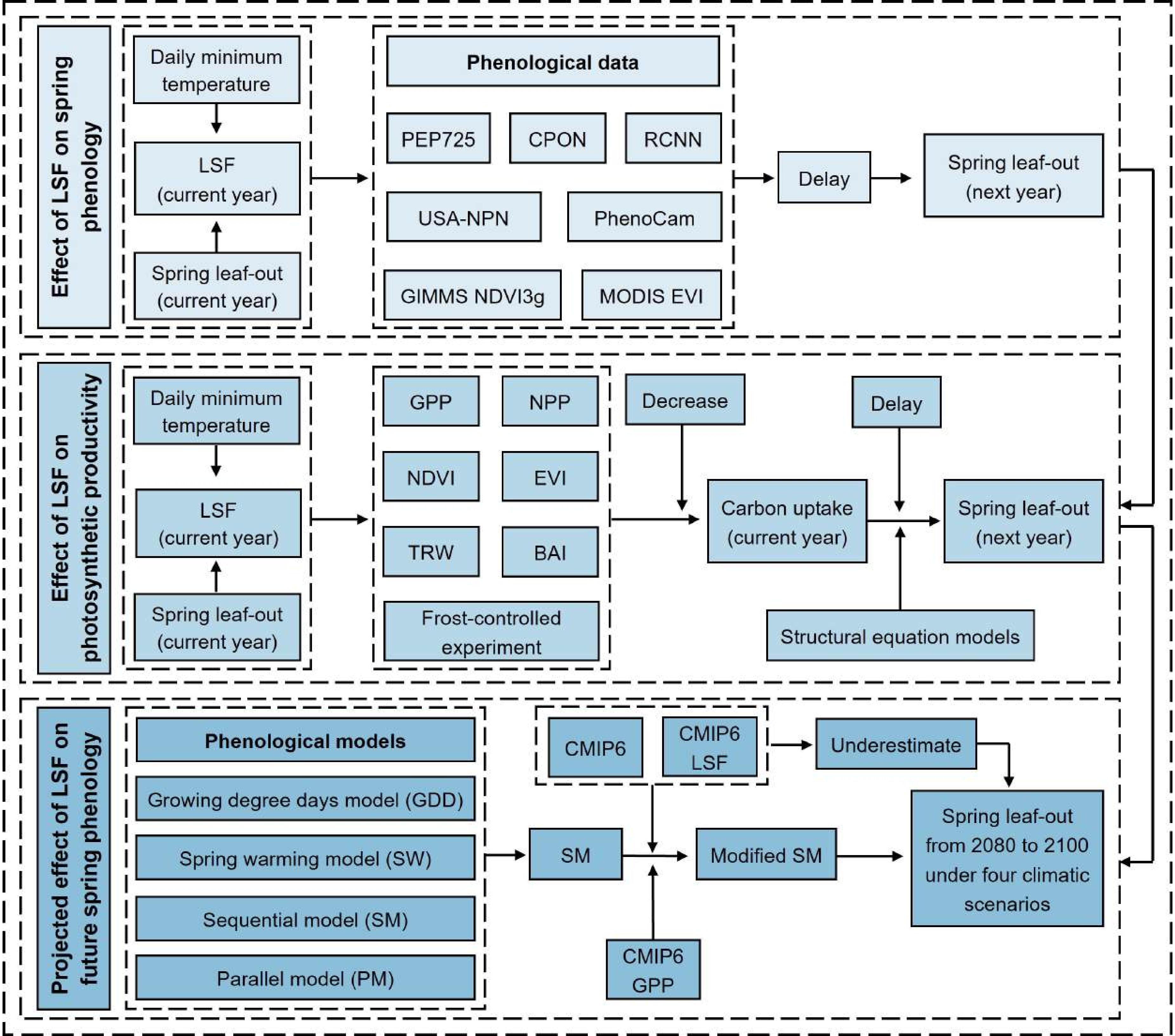
Effect of LSF on spring phenology
Daily minimum temperature
LSF (current year)
Spring leaf-out (current year)
Phenological data
PEP725
CPON
RCNN
USA-NPN
PhenoCam
GIMMS NDVI3g
MODIS EVI
Delay
Spring leaf-out (next year)
Effect of LSF on photosynthetic productivity
Daily minimum temperature
LSF (current year)
Spring leaf-out (current year)
GPP
NPP
NDVI
EVI
TRW
BAI
Frost-controlled experiment
Decrease
Carbon uptake (current year)
Delay
Spring leaf-out (next year)
Structural equation models
Projected effect of LSF on future spring phenology
Phenological models
Growing degree days model (GDD)
Spring warming model (SW)
Sequential model (SM)
Parallel model (PM)
CMIP6
CMIP6 LSF
Underestimate
SM
Modified SM
Spring leaf-out from 2080 to 2100 under four climatic scenarios
CMIP6 GPP